

GODDARD SPACE FLIGHT CENTER

Evaluation Report

"The information contained herein is presented for guidance of employees of the Goddard Space Flight Center. It may be altered, revised, or rescinded due to subsequent developments or additional test results. These changes could be communicated internally by other Goddard publications. Notice is hereby given that this document is distributed outside of Goddard as a courtesy only to other government agencies and contractors and is understood to be only advisory in nature. Neither the United States Government nor any person acting on behalf of the United States Government assumes any liability resulting from the use of the information contained herein."

Microcircuit (15)
Mfr.: IDT
P/N: 49C465
D/C: 9832

Malfunction Report

Purchase Specifications
commercial

Incoming Inspected

Screening Specifications
commercial

Project
EO-1
System
Parts testing
Requester
Bruce Meinhold (562)
Initiated Date
08/25/98
Investigator
A.Teverovsky (300.1)

Technical Approval/Date

Approval for Distribution/Date

Background

Fifteen Integrated Device Technology 49C465 microcircuits were submitted to the GSFC Parts Analysis Laboratory for an evaluation of their design and potential reliability concerns.

Part Description

The IDT 49C465 is a 32-bit flow-through error detection and correction unit. The part is encapsulated in a standard 144-terminal plastic quad flat package (PQFP).

Analysis

1. External and Radiographic Examinations

All samples were serialized (from SN 67 to SN 81) and subjected to external microscopic examination and radiography. Figure 1 gives an overall view of the part. Typical top and side X-ray views are shown Figures 2 and 3.

No package warping, cracks, voids, or foreign inclusions in the plastic encapsulant were found. No gaps were found between the leads entry and the molding compound. Radiographic examination showed adequate wire bond dressing. The die-paddle support bars had lead lock holes which enhanced a bond between the molding compound and the lead frame and increased moisture resistance of the part.

2. Scanning Acoustic Microscopy.

Top and bottom sides of all parts were examined using an acoustic microscope (C-SAM mode with a 30 MHz transducer). All parts had similar acoustic images. Typical images are shown in Figures 4 and 5. No abnormalities at the die-molding compound interface were noticed. Following analysis showed that a square frame on the lead frame was a polymer (most likely Kapton) tape used to support internal part of the leads. Red colors at the bottom view of the die paddle acoustic image indicate delamination at the die paddle-molding compound interface.

3. Internal Examinations

Six samples (SNs 76 through 81) were decapsulated in red fuming nitric acid and examined microscopically. Figure 6 shows an overall view of the part after decapsulation. Some bonding wires were exposed completely (both bonds to the die and to the lead frame). Small spots of bluish color at the exposed lead tips (see Figure 7) indicated an acid attack on a copper lead frame. No other defects were observed. Figures 8 and 9 give typical views of the dice after decapsulation and cleaning in oxygen plasma.

4. Bond Pull Test

All the wires in samples SN 76 and SN 78 were subjected to wire pull testing. The results are shown in Table 1. Both samples passed the test according to formal criteria of MIL-STD-883, TM 2011 (1.2 mil gold wires). Most of the completely exposed wires broke at the lead bond (BC 6) and had smaller pull forces compared to wires which broke at the neck (BC 1). The bonds to the lead frame were most likely weakened due to chemical attack during decapsulation. Two bonds in SN 78 separated along the ball-contact pad interface (BC2). As the pull force was high enough and no cratering was observed, this is not considered as a failure.

Table 1. Pull Test Statistics

Parameter	SN 76		SN 78		
	BC 1	BC 6	BC 1	BC 6	BC2
QTY	112	34	137	3	2
Min	9.3	7.8	9.0	3.0	11.0
Max	14.9	12.4	15.3	11.2	11.5
Average	11.7	10.15	11.45	8.2	
St. dev.	1.45	1.14	1.65	4.52	

5. SEM examination of glassivation and wire bonds

Bonds and glassivation in sample SNs 79 and 80 were inspected using a SEM. No glassivation defects were found (see Figure 10). Energy-dispersive X-ray microanalysis (EDX) indicated that the glassivation was composed of a nitride film. Cross section of the die (SN 76) revealed (see Figure 11) that the glassivation consisted of two layers: the first, most likely, was a silicon dioxide layer (approximately 0.15 μm) and the second was a silicon nitride/(oxynitride) film of approximately 0.7 μm of thickness.

Both parts had adequate wire-to-die bonding (see Figures 12, 13).

6. Glassivation Integrity

This examination was performed on samples SN 79 and SN 80 per MIL-STD-883D, Method 2021, "Glassivation layer integrity". The test involved a high power optical examination after the die was subjected to an aluminum etch. Multiple sites of aluminum corrosion were observed on both samples, mostly at the periphery of the dice. Figures 14 and 15 give typical SEM views of the failed sites. As no similar defects in the nitride films were seen before the glassivation integrity test, most likely they were created by a chemical attack on the aluminum metallization. Fine preexisting cracks (or pores) allowed acid attack on aluminum resulting in corrosion. Aluminum corrosion products have approximately three times the volume of pure aluminum, thus resulting in a swelling of the nitride film and widening of the cracks.

7. SEM inspection of metallization

The metallization was inspected in SN 81 per MIL-STD-883D, Method 2018 after glassivation removal. No patterning problems or other defects were found in top and bottom metallization layers. Metallization is shown in Figures 16, 17, and 18. The minimum line width was 1.2 μm . EDX analysis showed that Ti/W alloy (approximately 0.1 μ of thickness) was used as a metallization barrier layer. No void or thinning problems were observed with the Ti/W layer.

8. Cross Sectional Examinations

Two samples (SN 74 and SN 75) were cross sectioned at several planes and were examined using a high power optical microscope and a SEM.

8.1. Molding compound and lead frame.

The molding compound had no cracks or large voids and formed intimate contact to all internal surfaces (die, wires, and lead frame). Small spheres of a transparent material were probably silicone rubber additives used to reduce mechanical stresses.

The lead frame was made of copper of approximately 150 μm thick. Finger tips and the top of the die paddle were locally spot-plated with silver (approximately 5-7 μm thick). External parts of the lead frame were tinned.

A gap between the molding compound and the back side of the die paddle was observed in both parts in the central area of the pad. The gap width gradually increased toward the center of the die

paddle reaching several micrometers of thickness (see Figures 19 and 20). The gap widened to approximately 10 μm after the part had been heated to 70 °C for half an hour, then cooled to room temperature.

8.2. Die-to-molding compound interface.

No delaminations or gaps between the glassivation and the molding compound were observed.

8.3. Die integrity.

Both samples had longitudinal cracks along the silicon-oxide and/or oxide-metallization interfaces (see Figure 21). At the wire bond areas these cracks indicated cratering (see Figure 22). As no cratering was observed during the wire pull tests and no cracks were found during the bare die (SN 76) cross sectioning, these cracks were probably artifacts caused by the package cross sectioning.

8.4. Wire-to-lead frame and wire-to-die paddle bonds.

The gold wires formed adequate metallurgical contacts with the silver plating at all examined wire-to-lead frame bonds (see Figure 23).

Figure 24 gives an optical view and Figure 25 gives a SEM view of typical ball bond cross sections. Aluminum metallization under the contact pads was mostly consumed during bonding forming an Au/Al intermetallic layer (of light-gray color) 2 - 3 μm thick). No Kirkendall voiding was observed.

8.5. Die attachment.

The die was mounted to the lead frame base with a silver epoxy approximately 35 μm thick. The silver filler was uniformly distributed along the adhesive layer (see Figure 19). No delaminations or excessive voiding at the die attachment were found.

Discussion

1. Wire ball bonding.

Intermetallic formation at the ball-contact pad interface is normal and suggests a good metallurgical contact between the gold wires and aluminum metallization. Light-gray color of the intermetallic layer indicates normal low temperature Al/Au compounds. Due to a relatively thin (1 – 1.5 μm) layer of aluminum metallization, practically all the aluminum was consumed to form an intermetallic alloy. This may cause problems if the parts are used at elevated temperatures (more than 125 °C) for a long period of time, due to the possible formation of Kirkendall voids along the periphery of the bonds.

2. Die paddle-molding compound delamination.

This delamination, which was confirmed by acoustic microscopy and cross sectioning, is considered an indication of possible popcorning problem.

Molding compounds usually adhere to Alloy 42 better than to copper. However, the coefficients

of thermal expansion (CTE) for copper and molding compounds match each other better thus reducing thermomechanical stress and the possibility of delamination. Poor adhesion between the copper and the molding compound might be due to an excessive copper oxide film which usually grows during high temperature assembling processes (wire bonding and post mold curing).

A chemically roughened lead frame would adhere better to molding compound and reduce the risk of popcorning.

3. Cratering and longitudinal cracks.

It is known that the tendency to crater predominates in thin aluminum metallization. However, a hard titanium-tungsten underlayer should reduce the possibility of cratering. In this study, cratering and cracks along the die surface were revealed only when encapsulated parts were cross sectioned. These defects were not exposed during wire pull tests or cross sectioning of a bare die. One explanation assumes that the surface layers of an encapsulated silicon die are highly stressed and prone to crack formation and cratering. In that case, even minor mechanical disturbances during cross sectioning would be sufficient to cause fracturing.

4. Glassivation integrity.

The defects in glassivation were mostly found along the metallization lines at the periphery of the die. This can be explained by increased shearing stresses at the die edge. These stresses (caused by molding compound-die CTE mismatch) being applied to the glassivation “bumps” (along metallization lines) may have caused fine cracks which later developed under acid attack. A “bumpy” surface of glassivation significantly increases the possibility of crack formation. This possibility is usually minimized using a polyimide coating which enhances the interfacial integrity and provides surface planarization and stress relief. For example, a polyimide film 8 μm thick will reduce the failure rate by a factor of 3 during thermal shock test.

Conclusions

An evaluation of the Integrated Device Technology 49C465 microcircuits encapsulated in plastic packages revealed adequate die design and technology (good vias forming, metallization patterning and conformance, defect free Ti/W barrier layers). The molding compound had intimate contact with the die, wires, and leads. The die was properly mounted to the copper lead frame pad with a thin layer of silver epoxy. Interconnecting gold wires had good alignment, deformation and dressing. The parts passed wire pull test per MIL-STD-883, TM 2011. Both bonds (to contact pads and to leads) formed adequate metallurgical contacts.

The thickness of the Au/Al intermetallic was 1-3 μm and the aluminum under the bonds was mostly consumed. This may cause some bond integrity problems during a long term aging/operation at elevated temperatures.

Cross sectioning of encapsulated dice exposed cratering under contact pads and cracks along the silicon-oxide and/or oxide-metallization interfaces. Although these defects were most likely

artifacts caused by cross sectioning, they indicate high mechanical stresses in the die and a tendency to form cracks.

Delamination between the bottom side of the die paddle and the molding compound was revealed during acoustic microscopy and cross sectioning. Similar defects increase the risk of popcorning during surface mounting.

Rejectable defects (per MIL-STD-883, TM 2021) were observed along the periphery of the die during the glassivation integrity test. The lack of polyimide conformal coating, which is commonly used in similar parts, probably resulted in increased mechanical stresses and caused cracking of the silicon nitride glassivation layer.

To ensure the quality of the parts, additional analysis of their thermomechanical robustness, including SMT simulation tests and multiple thermal cycles/thermal shocks are recommended.



Figure 1. An overall view of the microcircuit.

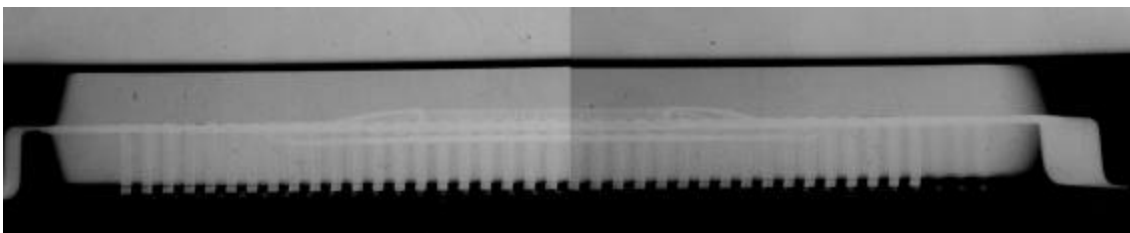


Figure 2. Side X-ray view of the package. (6X)

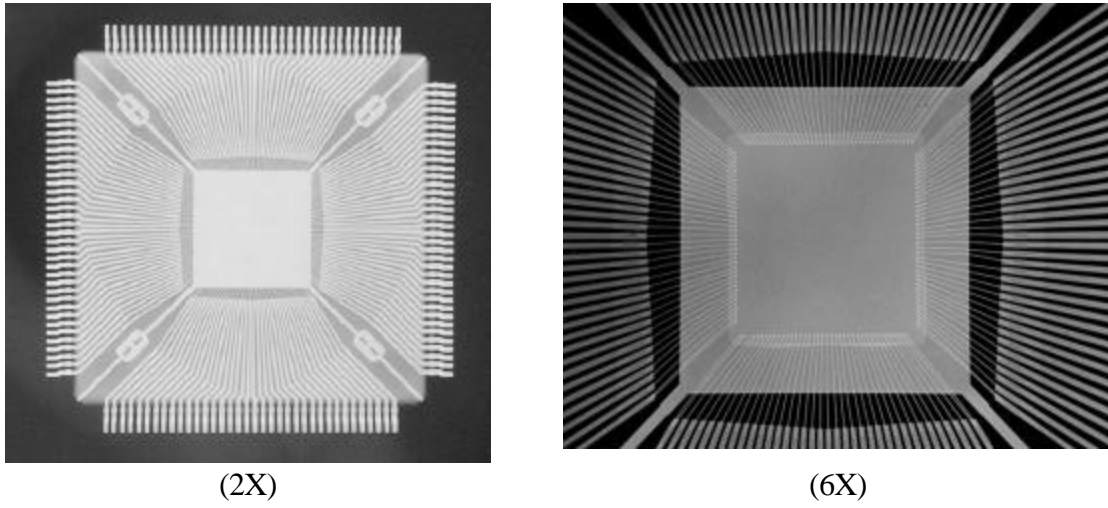


Figure 3. Top X-ray views of the microcircuit. Note good wire dressing.

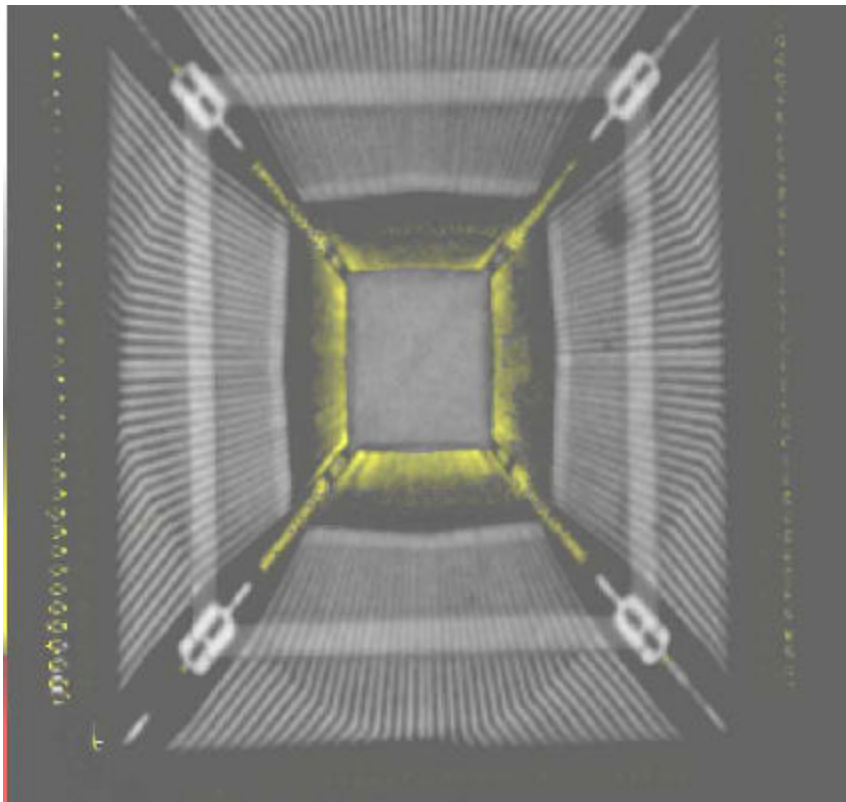


Figure 4. Typical acoustic image of the part. Top view, SN 78.

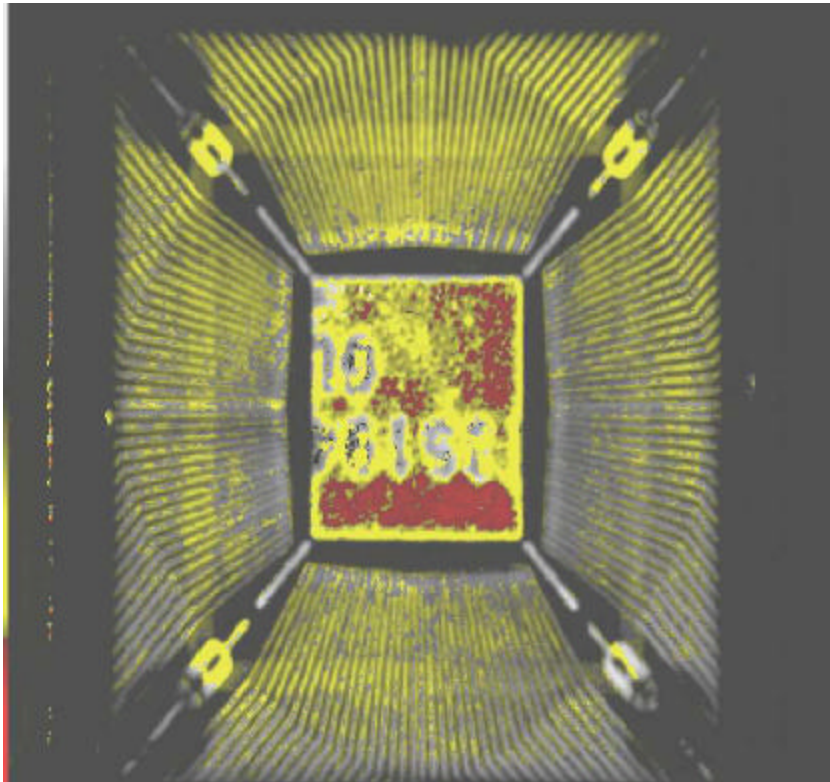


Figure 5. Typical acoustic image of the part. Bottom view, SN 81. Red color indicates delamination.

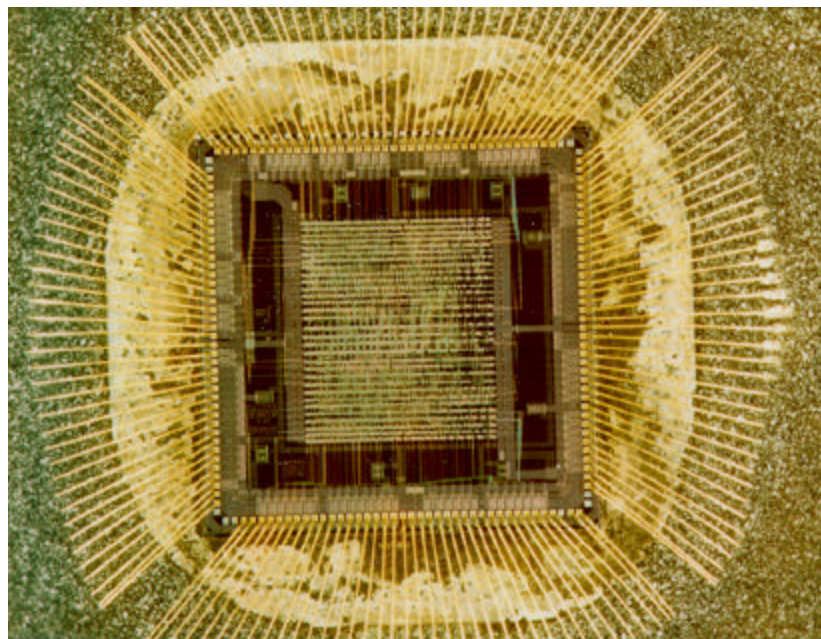


Figure 6. Overall view of the microcircuit after decapsulation, SN 79. (8X)



Figure 7. Close up internal view showing products of the acid attack on exposed copper leads, SN 77. (16X)

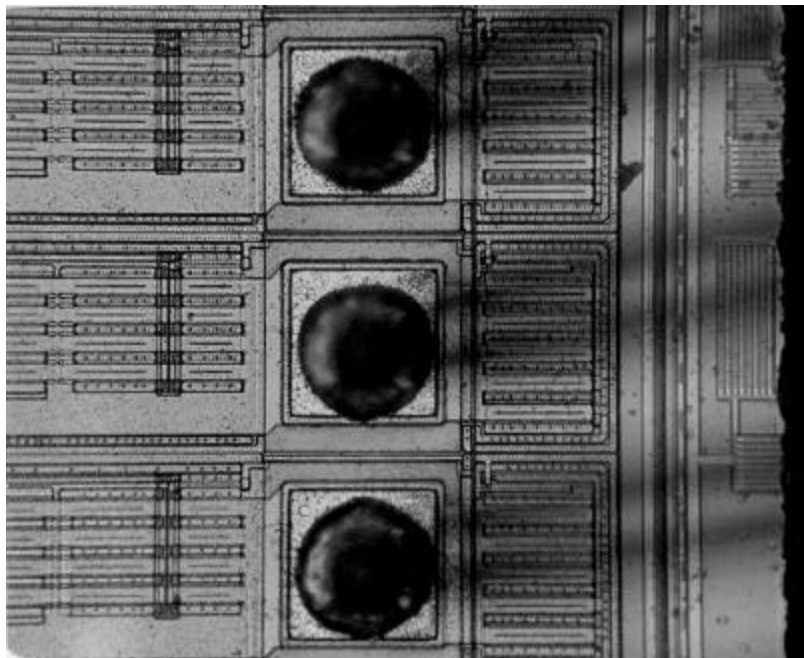


Figure 8. Optical internal view showing typical ball bond alignment, SN 80 (200X)

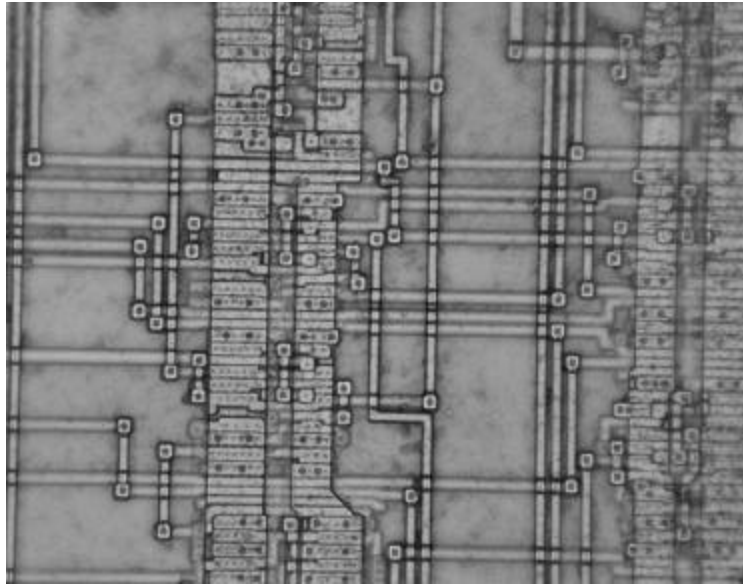


Figure 9. Optical view of the die metalization showing good patterning, SN 81. (500X)

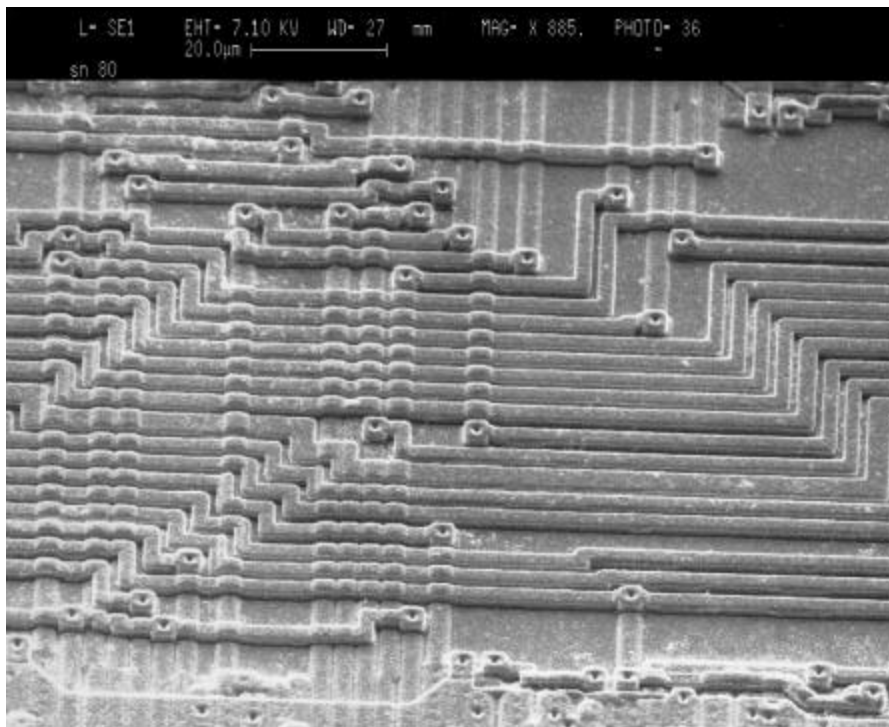


Figure 10. Typical SEM view of the die glassivation showing adequate coverage of the metallization.

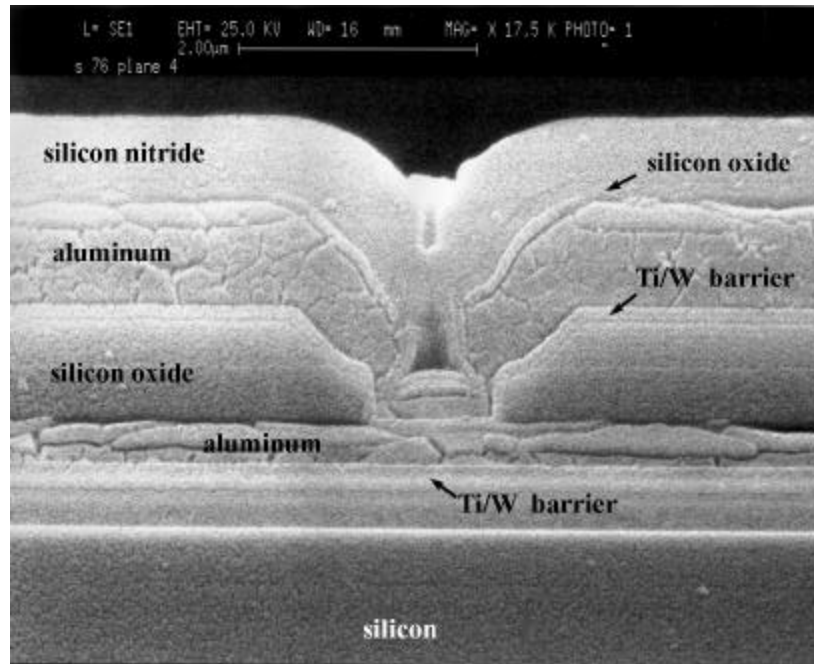


Figure 11. SEM view of the die cross section indicating features of the die technology.

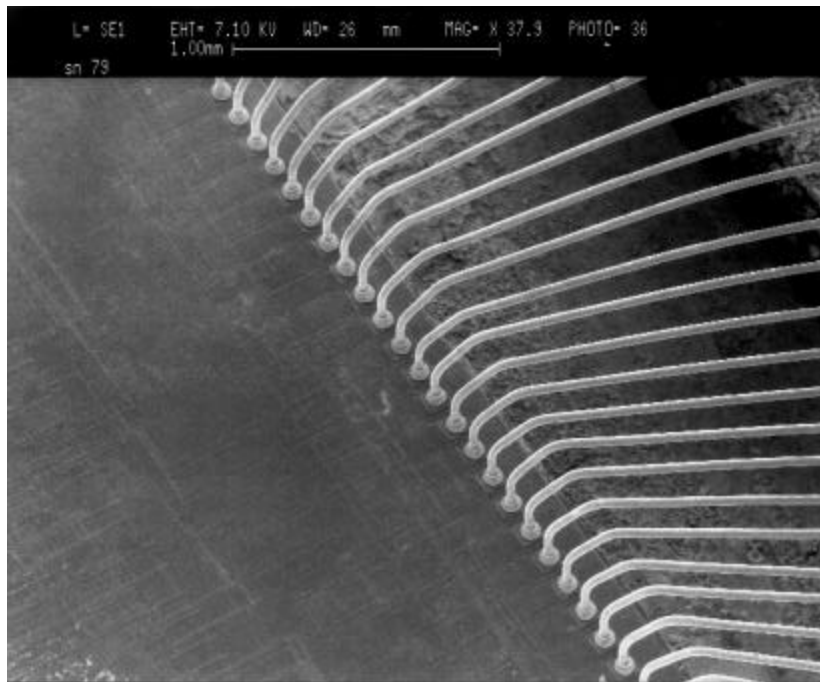


Figure 12. Typical SEM view of wire bond alignment and dressing.

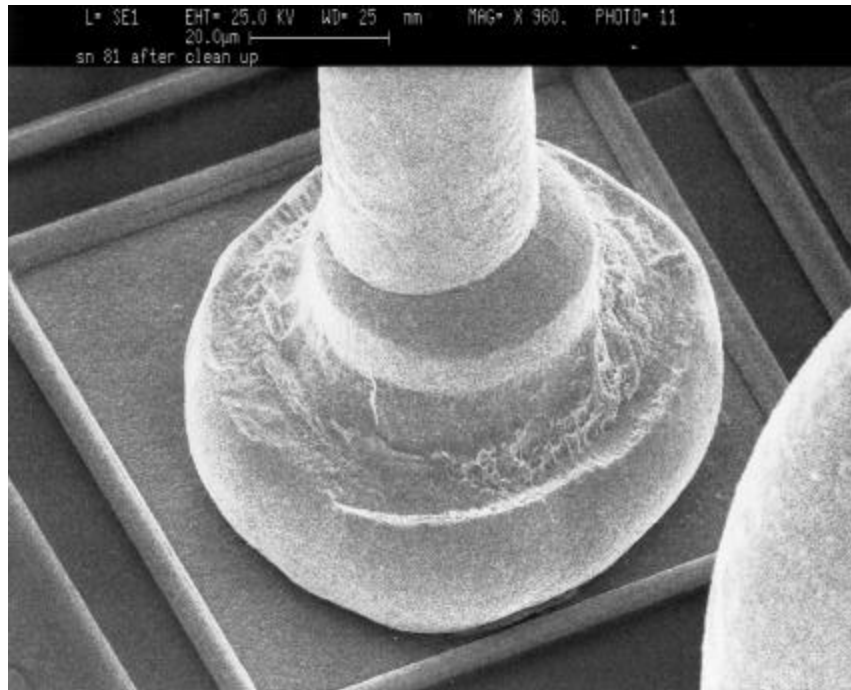


Figure 13. Typical SEM view of a wire ball bonding showing good deformation and placement.

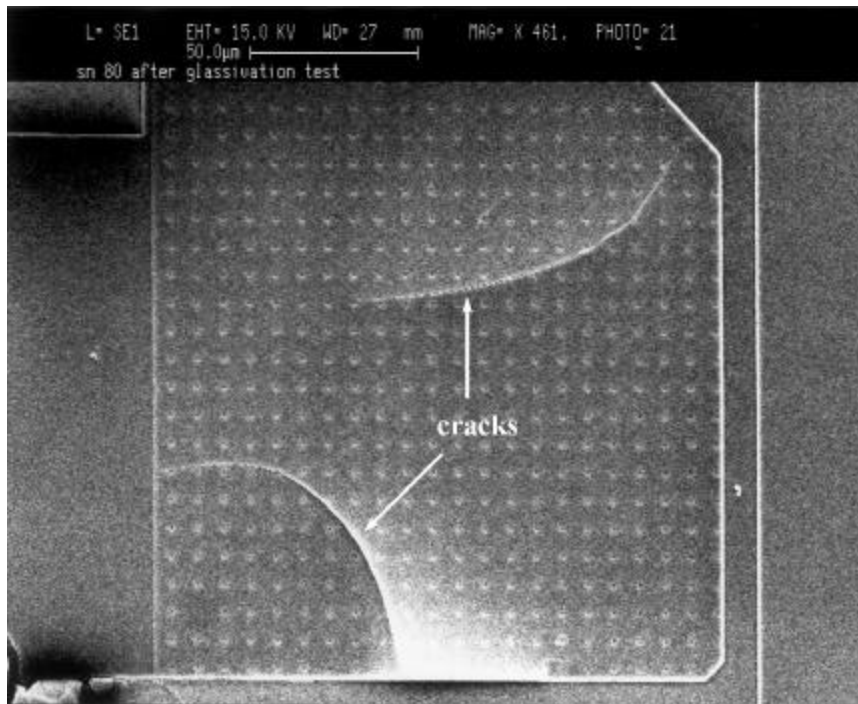


Figure 14. Cracks and peeling of the silicon nitride film after glassivation integrity test.

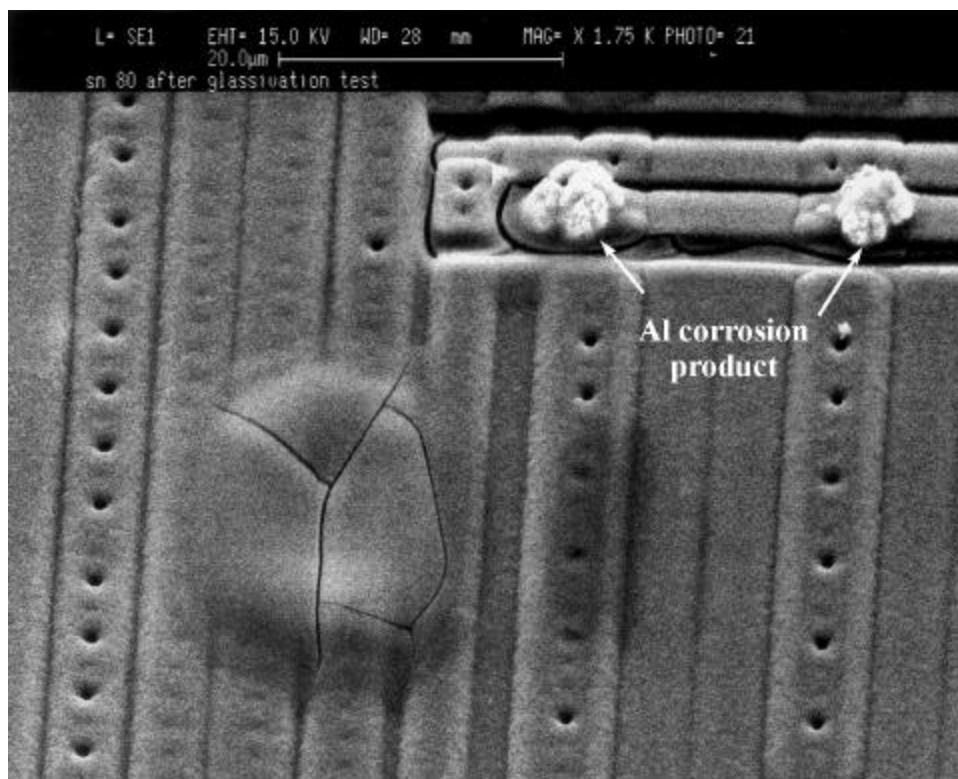


Figure 15. Typical defects revealed during the glassivation integrity test.

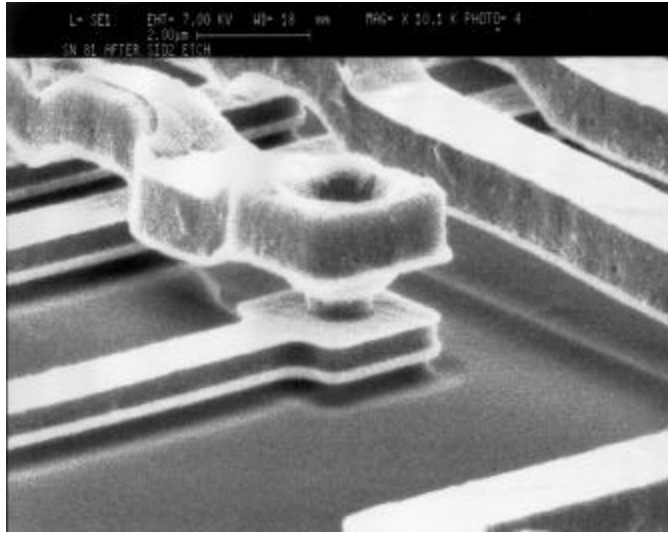


Figure 16

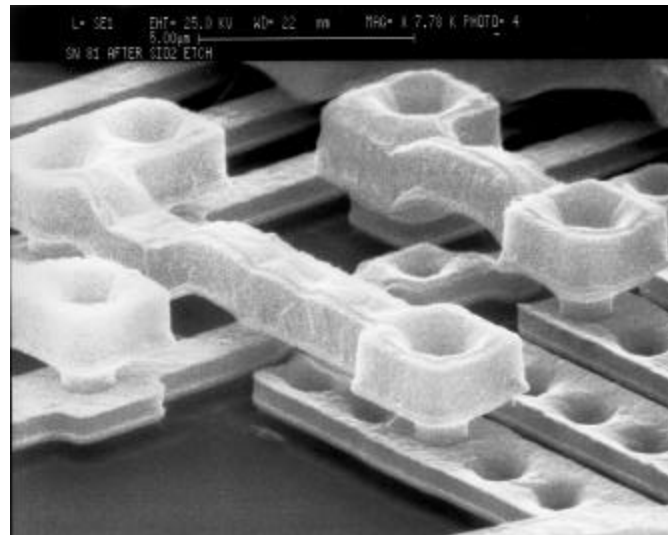


Figure 17

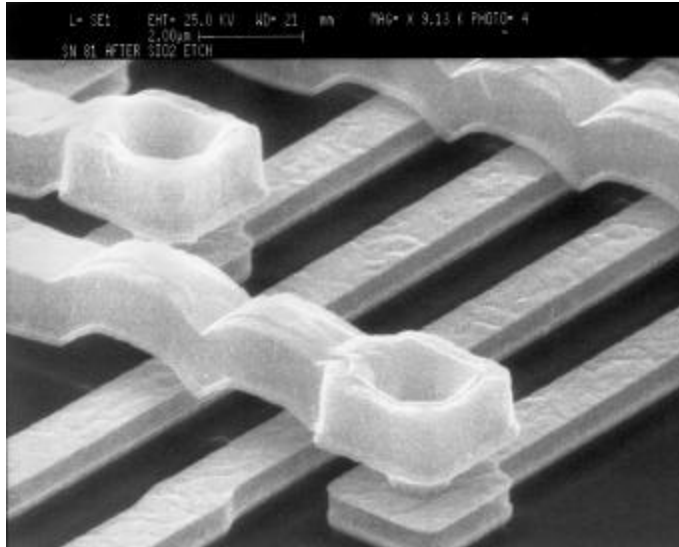


Figure 18

Figures 16 - 18. Typical SEM views of the top and bottom metallization.

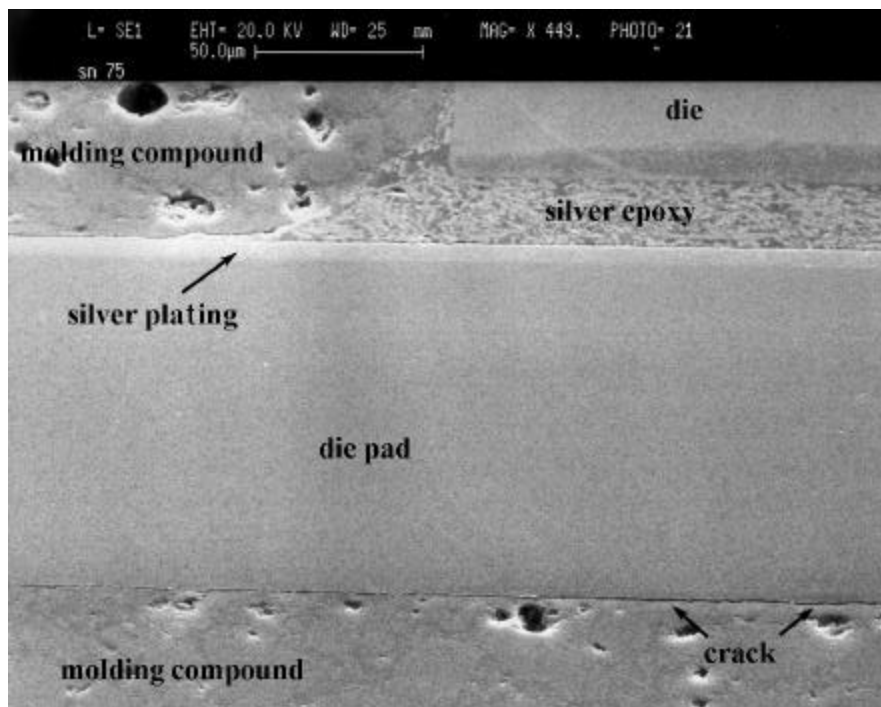


Figure 19

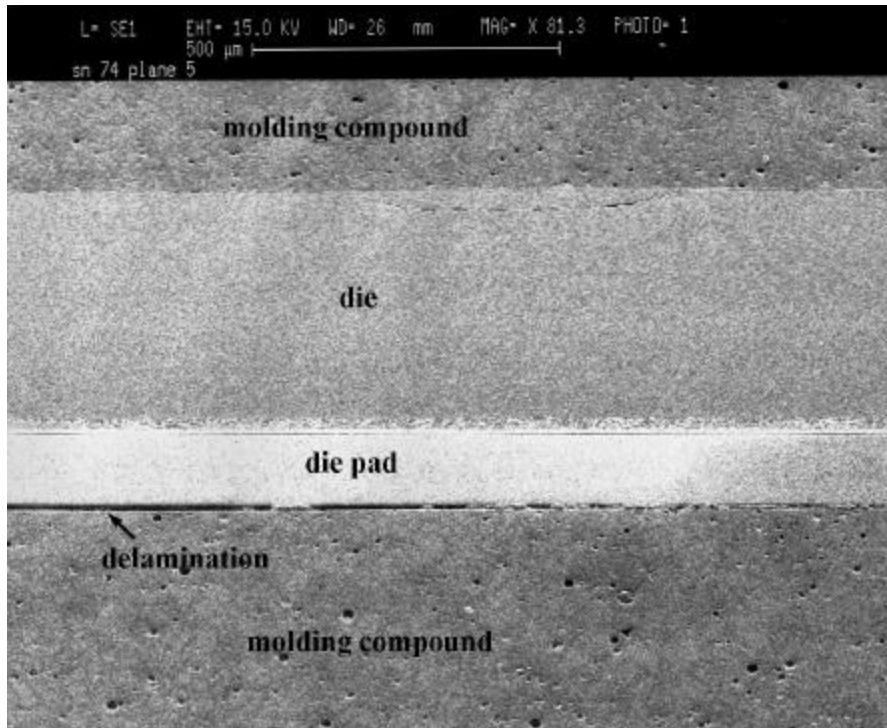


Figure 20

Figures 19-20. SEM views of cross sections showing gaps between the die pad and molding compound.

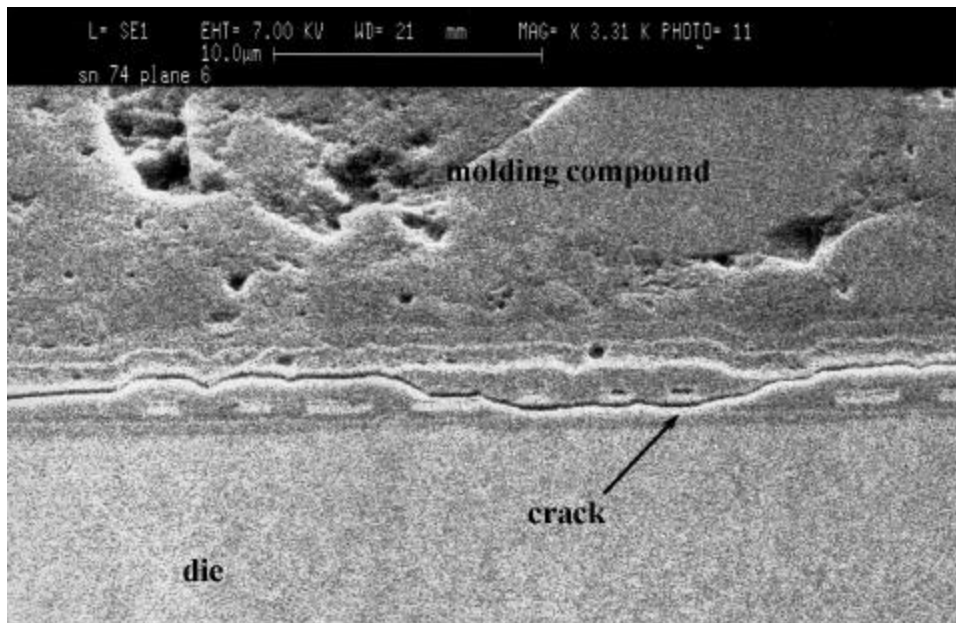


Figure 21. SEM view of the crack along the die surface. Similar cracks were observed at all cross sections of the parts.

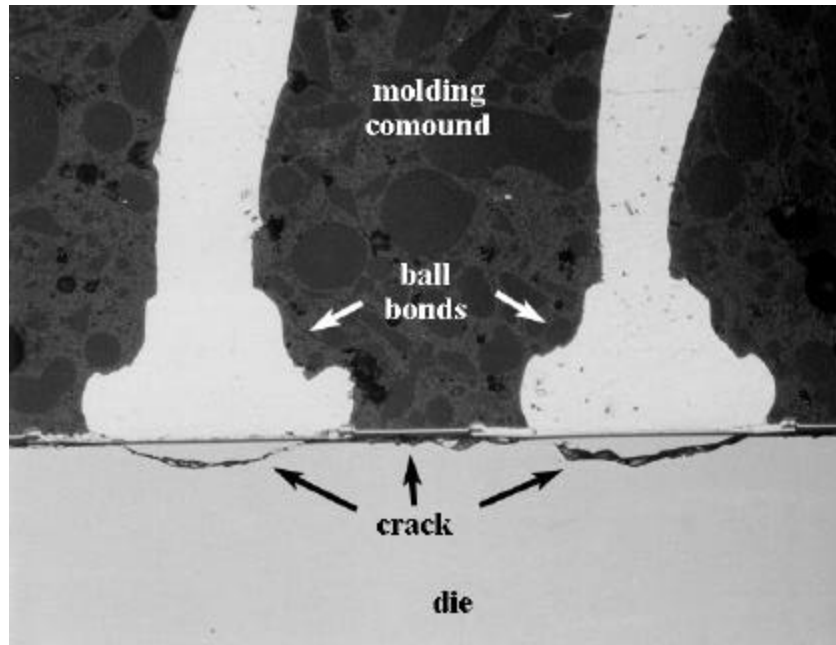


Figure 22. Optical view of the wire-to-contact pad cross section, SN 75. The cracks indicate possible cratering problems. (920X).

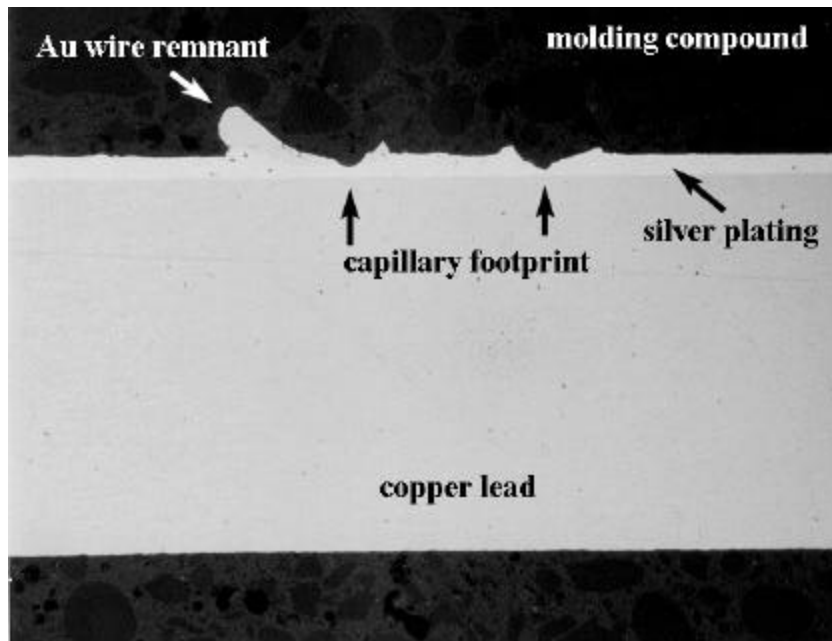


Figure 23. Optical view of the wire-to-lead bond cross section, showing adequate deformation at stitch bonds, SN 75. (400X)

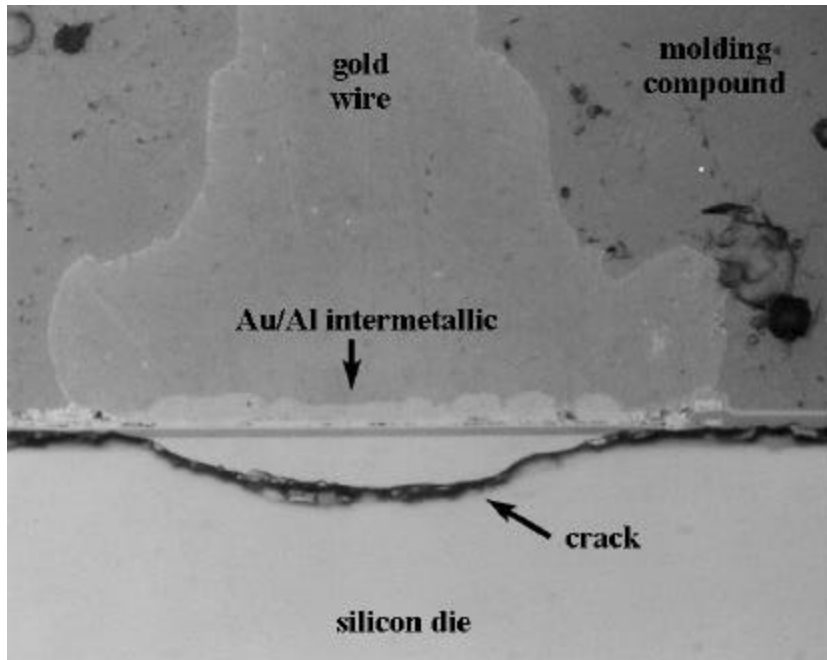


Figure 24. Optical view of a wire-to-die ball bond showing intermetallic at the bond interface, SN 75. (1000X)

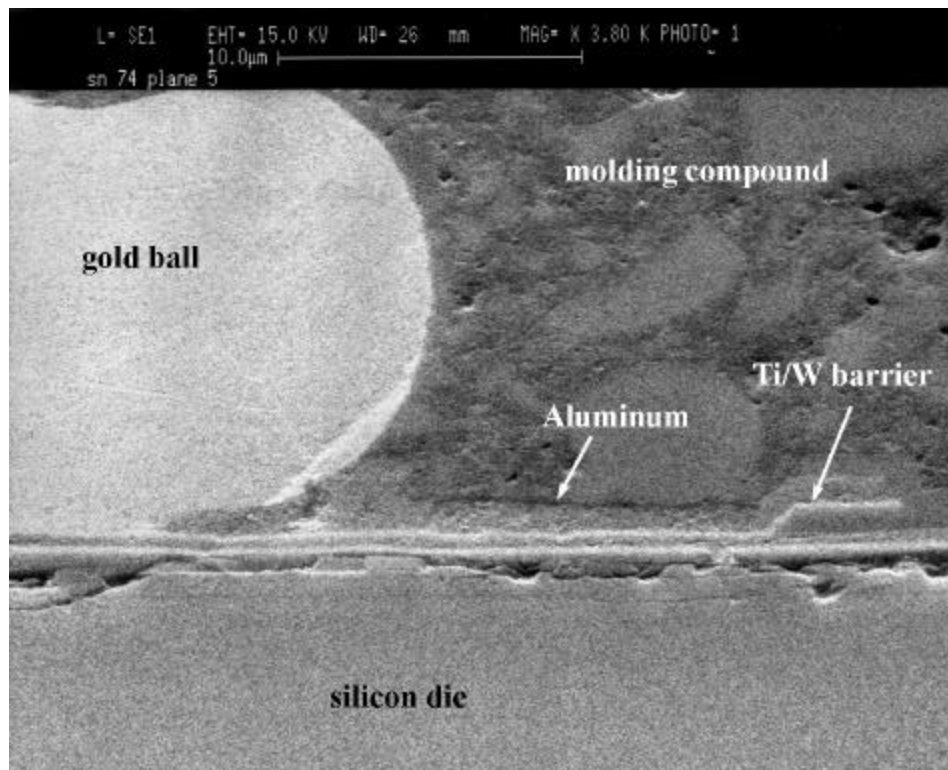


Figure 25. SEM view of the ball bond-to-die cross section.